Published online April 23, 2004

Nucleic Acids Research, 2004, Vol. 32, No. 7 ***2193–2201***
DOI: 10.1093/nar/gkh556

XRCC1 co-localizes and physically interacts with PCNA

Jinshui Fan, Marit Otterlei[1], Heng-Kuan Wong, Alan E. Tomkinson[2] and David M. Wilson III*

Laboratory of Molecular Gerontology, National Institute on Aging, 5600 Nathan Shock Drive, Baltimore, MD 21224, USA, [1]Department of Cancer Research and Molecular Medicine, Norwegian University of Science and Technology, N-7489, Trondheim, Norway and [2]Radiation Oncology Research Laboratory, Department of Radiation Oncology and Greenbaum Cancer Center, University of Maryland Medical Center, 655 West Baltimore Street, Baltimore, MD 21201, USA

Received March 8, 2004; Revised and Accepted March 30, 2004

ABSTRACT

X-ray Repair Cross Complementing 1 (XRCC1) is thought to function as a scaffolding protein in both base excision repair and single-strand break repair (SSBR), since it interacts with several proteins participating in these related pathways and has no known enzymatic activity. Moreover, studies indicate that XRCC1 possesses discrete G_1 and S phase-specific functions. To further define the contribution of XRCC1 to DNA metabolism, we determined the *in vivo* localization pattern of this protein and searched for novel protein interactors. We report here that XRCC1 co-localizes with proliferating cell nuclear antigen (PCNA) at DNA replication foci, observed exclusively in the S phase of undamaged HeLa cells. Furthermore, fluorescence resonance energy transfer (FRET) analysis and co-immunoprecipitation indicate that XRCC1 and PCNA are in a complex and likely physically interact *in vivo*. *In vitro* biochemical analysis demonstrated that these two proteins associate directly, with the interaction being mediated by residues between amino acids 166 and 310 of XRCC1. The current evidence suggests a model where XRCC1 is sequestered via its interaction with PCNA to sites of DNA replication factories to facilitate efficient SSBR in S phase.

INTRODUCTION

The Chinese hamster ovary (CHO) mutant EM9 was originally isolated on the basis of increased sensitivity to the alkylating agent ethyl methanesulfonate (EMS) and was concurrently shown to be cross-sensitive to ionizing radiation (1). Following exposure to these DNA-damaging agents, the rate of single-strand break (SSB) rejoining was found to be impaired several fold, indicating a defect in DNA repair. EM9 cells also exhibit a very high level (elevated ~10-fold) of sister chromatid exchange (SCE), particularly when grown in the presence of bromodeoxyuridine (BrdU) or chlorodeoxyuridine (CldU). It was hypothesized that once incorporated, these halogenated bases are incompletely processed by the repair machinery in EM9, leading to the formation and accumulation of recombinagenic DNA strand break intermediates (2). The gene defective in these mutant cells was later identified in a screen for genomic fragments that confer resistance to CldU treatment (3). Since the initial effort was to isolate X-ray repair genes, the cross-complementing human gene was termed X-ray Repair Cross Complementing 1.

There is substantial biochemical evidence indicating that XRCC1 participates in base excision repair (BER) and single-strand break repair (SSBR). XRCC1 was first found to physically associate with DNA ligase IIIα (LIG3α), an enzyme that functions to seal single-strand nicks in DNA (4). EM9 cells possess lower than normal levels of LIG3α protein, indicating that XRCC1 functions to stabilize this *in vivo* partner. Since this initial discovery, several other studies have reported interactions between XRCC1 and proteins involved in BER and SSBR. For instance, XRCC1 has been shown to interact with DNA polymerase β (POLβ) (5–7), apurinic endonuclease (APE1) (8), polynucleotide kinase/phosphatase (PNKP) (9), tyrosyl DNA phosphodiesterase (TDP1) (10), poly (ADP-ribose) polymerases 1 and 2 (PARP1/2) (5,11,12) and 8-oxoguanine DNA glycosylase (OGG1) (13). Although no catalytic function has been ascribed to XRCC1, nick, gap and double-strand break (DSB) DNA binding activities have been associated with this protein (7,14).

While both biological and biochemical evidence indicates a direct role for XRCC1 in BER/SSBR, likely as a scaffolding protein via the interactions noted above, other studies have suggested functions for XRCC1 in DNA replication and/or recombination. In particular, Taylor *et al*. (15) found that EM9 cells expressing a mutant form of XRCC1, which is defective in its ability to interact with LIG3α through its C-terminal

*To whom correspondence should be addressed. Tel: +1 410 558 8153; Fax: +1 410 558 8157; Email: wilsonda@grc.nia.nih.gov

The authors wish it to be known that, in their opinion, the first two authors should be regarded as joint First Authors

BRCT (BRCA1 C-terminal) domain (BRCT2), are deficient in SSBR during G_1 phase yet proficient in SSBR during S phase. This finding suggested cell cycle-specific roles for XRCC1, where the XRCC1–LIG3α interaction is required for G_1 SSBR, but is dispensable for this process in S phase. Moreover, Kubota and Horiuchi (16) reported that mutation of the central BRCT domain (BRCT1), but not BRCT2, results in a protein that is unable to restore alkylating agent resistance to EM9 cells. They subsequently found that XRCC1 mutant cell lines expressing XRCC1 with a mutated BRCT1 domain exhibit normal SSBR activity, but suffer from a defective reinitiation of replication following methyl methanesulfonate (MMS) challenge. This finding is generally consistent with the observations of Taylor *et al.* (17), who reported that the BRCT1 domain of XRCC1 is required for proficient repair during both the G_1 and S/G_2 cell cycle phases. Taylor *et al.* (15) also found that XRCC1 partially co-localizes with Rad51, implying a role for XRCC1 in homologous recombination-related processes. Thus, evidence indicates that XRCC1 has distinct functions in the G_1 and S phases, with potential roles in replication and/or recombination.

To further explore the contributions of XRCC1 to DNA metabolism, we determined the *in vivo* localization patterns of this protein using fluorescently tagged XRCC1 proteins. We report here that XRCC1 localizes to sites of replication foci, independent of exogenous DNA damage, and interacts directly with PCNA both *in vivo* and *in vitro*, revealing a novel molecular link between XRCC1-mediated responses and chromosomal DNA replication.

MATERIALS AND METHODS

Fluorescently tagged protein expression systems

To generate the yellow fusion protein (YFP)-tagged XRCC1 expression constructs, human *XRCC1* cDNA was first PCR amplified. Oligonucleotide primers 5′X1BlgN (gaagatctcaccatgccggagatccgcctccg) and 3′XEcoN (cggaattcgggcttgcggcaccaccccat) were used to generate the *XRCC1* fragment subcloned into the pEYFP-N1 vector (Clontech). The PCR product was digested with BlgII and EcoRI and incorporated into the identical sites within pEYFP-N1 to create pXRCC1-EYFP, which expresses YFP as a C-terminal tag to XRCC1. Primers 5′X1BglC (gaagatctatgccggagatccgcctccg) and X13′Eco (ctaggaattctcaggcttgcggcaccaccc) were used to amplify the *XRCC1* fragment, which was subcloned into the BlgII and EcoRI sites of pEYFP-C1 to create the N-terminal YFP-tagged pEYFP-XRCC1 plasmid. XRCC1 constructs expressing a cyan fusion protein (CFP) were generated exactly as above, except the *XRCC1* PCR fragment was subcloned into the BlgII and EcoRI restriction sites of the appropriate pECFP vector (Clontech). The pECFP-PCNA, pUNG2-ECFP (which encodes a uracil-DNA glycosylase fusion protein) and pUNG2-EYFP plasmids have been described previously (18).

Confocal microscopy and FRET measurements

HeLa S3 cells transfected with pXRCC1-EYFP were typically cultured in DMEM containing fetal calf serum, garamycin (100 μg/ml), glutamine and geneticin G418 (400 μg/ml) (Invitrogen). Untransfected HeLa cells were cultured in the same medium without geneticin. Cells were transfected using a $CaPO_4^-$ method (Profection; Promega) according to the manufacturer's recommendations. To view fluorescent images of living cells (1 μm thickness), a Zeiss LSM 510 laser scanning microscope equipped with a Plan-Apochromate 63×/1.4 oil immersion objective was used. FRET was determined by modifying the general equations of Matyus (19), for use with the ECFP and EYFP fusion proteins designated as donor (D) and acceptor (A), respectively. FRET occurs if $I_2 - I_1[I_{D2}/I_{D1}] - I_3[I_{A2}/I_{A3}] > 0$, where I represents the intensities in three channels given in arbitrary units (20). Intensities were measured as follows: channel 1, $I_{1,\ A1,\ D1}$, excitation at $\lambda = 458$, detection at 480 nm $< \lambda >$ 520 nm (ECFP); channel 2, $I_{2,\ D2,\ A2}$, excitation at $\lambda = 458$ nm, detection at $\lambda > 560$ nm; channel 3, $I_{3,\ D3,\ A3}$, excitation at $\lambda =$ 514 nm, detection at $\lambda > 560$ nm (EYFP). $I_{D1,\ D2,\ D3}$ and $I_{A1,\ A2,\ A3}$ were determined accordingly for cells transfected with only ECFP and EYFP fusion proteins with the same settings and at the same levels of fluorescence intensities (I_1 and I_3) as for the co-transfected cells. FRET values were normalized to account for differences in the respective fluorochrome expression levels using the following equation: normalized FRET ($FRET_N$) = $FRET/(I_1 \times I_3)^{1/2}$ (21).

Immunoprecipitation assays

Once harvested, 293T cell pellets were washed with 1× phosphate-buffered saline (PBS), resuspended in buffer A (1× PBS, 1% Nonidet P-40, 0.5% sodium deoxycholate, 0.1% SDS) containing 0.5 mM pheylmethylsulfonyl fluoride (PMSF) and Complete® protease inhibitor cocktail (one tablet in 50 ml of buffer) (Roche) and sonicated. Following sonication, 5 U DNase I (Sigma-Aldrich) was added and the mixture was incubated at room temperature for 1 h and 4°C for 3 h. After centrifugation (10 000 *g*, 10 min), the supernatant was saved as 'whole cell extract' and the protein concentration was determined using the Bio-Rad protein assay (bovine serum albumin as standard). For immunoprecipitation, whole cell extract (~500 μg protein) was incubated at 4°C overnight with 2–4 μg anti-PCNA antibody (P-10; Santa Cruz Biotechnology), followed by incubation at 4°C for 3 h in the presence of 20 μl of rG protein–agarose beads (Invitrogen). The beads were washed three times with buffer A and were subsequently incubated at 90°C for 5 min in 30 μl of SDS protein gel loading dye and subjected to standard SDS–PAGE. XRCC1 and PCNA were detected by western blotting using anti-XRCC1 (4421-MC-100; Trevigen) or the anti-PCNA antibody above as per the manufacturer's recommendations.

HeLa cells stably transfected with XRCC1–EYFP and EYFP were harvested by centrifugation from exponentially growing cells in suspension and the cell pellet was immediately frozen in liquid nitrogen. All the succeeding steps were performed with ice-cold buffers. The cells were resuspended in an equal volume of 1× packed cell volume (PCV) buffer I (10 mM Tris–HCl, pH 7.8, 200 mM KCl) and 1× PCV buffer II [10 mM Tris–HCl, pH 8.0, 200 mM KCl, 40% v/v glycerol, 0.5% Nonidet P-40, 2 mM dithiothreitol (DTT), Complete® protease inhibitor, 1 mM PMSF]. Omnicleave™ Endonuclease (Epicentre) was added at 200 U/800 μl cell suspension. The cells were briefly sonicated and examined for cell disruption by microscopy and the protein concentration was determined as above. The cell extracts were snap frozen in liquid nitrogen and stored in aliquots at –80°C. For each

Table 1. Recombinant constructs that express full-length XRCC1 or a protein fragment

Construct	Primers (5′→3′) used for amplification	Residues included	Restriction sites for cloning	Protein tag(s)
XRCC1-pET29a	CGGAATTCATGCCGGAGATCCGCCTC AGGAGAATGCGGCCGCGGCTTGCGGCACCACCCCAT	1–633	EcoRI and NotI	N-terminal S tag, C-terminal HIS tag
NTD-pET16b	GGAATTCCATATGCCGGAGATCCGCCTCCG CGGGATCCTCACTCATCTTTGTCTGGG	1–157	NdeI and BamHI	N-terminal HIS tag
XNTD-pET16b	GGAATTCCATATGCCGGAGATCCGCCTCCG CGGGATCCTCATCGGGGTCGTCTGGGCTCGGT	1–310	NdeI and BamHI	N-terminal HIS tag
MD-pET16b	GGAATTCCATATGGTGACAGTGACCAAGCTTG CGGGATCCTCATTTGGTCTGGGGTTGCTTCT	166–436	NdeI andBamHI	N-terminal HIS tag
BLB-pET28a	GGAATTCCATATGGCTGGCCCAGAGGAGCTGGG CTAGGAATTCTCAGGCTTGCGGCACCACCC	311–633	NdeI and EcoRI	N-terminal HIS tag
BRCT2-pET28a	GGAATTCCATATGGAGCTCCCAGATTTCTTCCA CTAGGAATTCTCAGGCTTGCGGCACCACCC	538–633	NdeI and EcoRI	N-terminal HIS tag

Construct names are indicated in the first column and incorporate the pET vector backbone (Novagen). The N-terminal (top) and C-terminal (bottom) amplification primers are shown in column 2, with the subcloning sites indicated in the fourth column. The amino acid residues of XRCC1 included into the final protein expression product are denoted in column three and associated tags are indicated in the final column. S tag, S·Tag peptide sequence; HIS tag, polyhistidine sequence tag.

immunoprecipitation ~500 µg cell extract was diluted to 300 µl with an equal volume of buffer I and II containing 5 mM $MgCl_2$ and 200 U Omnicleave™ Endonuclease. The cell lysates were incubated at 4°C overnight with anti-GFP antibody (ab290; Abcam) covalently linked to protein A beads (according to the manufacturer's procedure). After washing three times with 0.5 ml of 1:1 buffer I:buffer II, the beads were resuspended in 15 µl of Nupage loading buffer (Invitrogen), heated and run on a 4–15% SDS ready Tris–HCl Nupage gel. Proteins were transferred to a PVDF membrane (Immobilon™; Millipore) and detected by western blotting using the antibodies noted above.

Recombinant XRCC1 proteins

DNA for XRCC1 and its five fragments was amplified from the wild-type human *XRCC1* cDNA (a gift from Dr Larry Thompson) using the primers listed in Table 1. The amplified DNA was cloned into a pET vector (Novagen), such that all the recombinant proteins were histidine (HIS) tagged at the N-terminus, excluding full-length *XRCC1*, which was both S peptide and HIS tagged at the N- and C-termini, respectively (Table 1). The cloned DNA was sequenced to ensure that the encoded proteins were free of mutation.

The recombinant plasmids were transformed into *Escherichia coli* strain BL21 (λDE3) for protein expression. Protein purification followed the procedure described by Caldecott *et al*. (5), with some modifications. All procedures were performed at 4°C unless otherwise indicated. Briefly, bacterial cells were grown at 37°C to a density of $OD_{600} = 0.6$–1.2 and isopropyl β-D-thiogalactopyranoside was added to 1 mM to induce protein expression. Cells were harvested 3 h after induction. Cells from a 2 l culture were resuspended in 50 ml of sonication buffer (50 mM HEPES–NaOH, pH 8.0, 0.5 M NaCl, 0.1 mM EDTA, 10% glycerol) and frozen at –80°C overnight. After the cell suspension was thawed, imidazole, PMSF and DTT were each added to a final concentration of 1 mM. Cells were disrupted by sonication and the lysate was centrifuged (14 000 *g*, 20 min). The supernatant was then mixed with 3 ml of Ni–NTA–agarose (Novagen) and stirred for 1 h. The suspension was applied to a 20 ml dispensable column (Bio-Rad), which was subsequently washed with 50 ml of sonication buffer, followed by additional washing/elution with 30, 15 and 15 ml of wash buffer (50 mM HEPES–NaOH, pH 8.0, 0.1 M NaCl, 0.1 mM EDTA, 1 mM DTT, 10% glycerol) containing 40, 80 and 250 mM imidazole, respectively. The fractions containing XRCC1 or its fragments were dialyzed against dialysis buffer (50 mM HEPES–KOH, pH 7.5, 150 mM KCl, 0.02 mM EDTA, 1 mM DTT, 10% glycerol) and concentrated with Centriprep (Millipore).

In vitro protein interaction assays

Purified N-terminal S peptide-tagged, full-length XRCC1 (4 µg) was incubated with 2 µg of the protein of interest (POLβ, APE1, FEN1 or PCNA) in 50 µl of binding buffer (50 mM HEPES–KOH, pH 7.5, 150 mM KCl, 0.015% Triton X-100, 0.02 mM EDTA, 1 mM DTT, 10% glycerol) on ice for 30 min. The mixture was transferred to a microcentrifuge tube containing 8 µl of S protein–agarose (Novagen). After being kept on ice for 1 h with constant stirring, the S protein–agarose was pelleted and washed four times with 200 µl of binding buffer. The S protein–agarose was finally resuspended in 20 µl of SDS protein gel loading dye, incubated at 90°C for 10 min and loaded onto a 12% polyacrylamide–SDS gel. After electrophoresis, the proteins were visualized by silver staining (Bio-Rad). Purified human recombinant untagged PCNA (22), APE1 (23), POLβ (24) and FEN1 (25) proteins were isolated as described.

The protocol of Kubota *et al*. (6) was adapted for the interaction assay of XRCC1 or one of its fragments with PCNA. The various XRCC1 proteins (2 µg) were incubated with PCNA (2 µg) in 25 µl of dialysis buffer (see above) containing 0.5 µg BSA on ice for 30 min. Ni–NTA–agarose (3 µl) was then added and after 1 h on ice with constant stirring, the agarose was washed five times with 200 µl of dialysis buffer containing 25 mM imidazole. Proteins were eluted from the agarose by addition of SDS protein gel loading dye (20 µl), followed by incubation at 90°C for 10 min. After electrophoresis of the supernatant, proteins were transferred to a PVDF membrane (Bio-Rad) and western blot analysis was performed using anti-PCNA antibody (P-10).

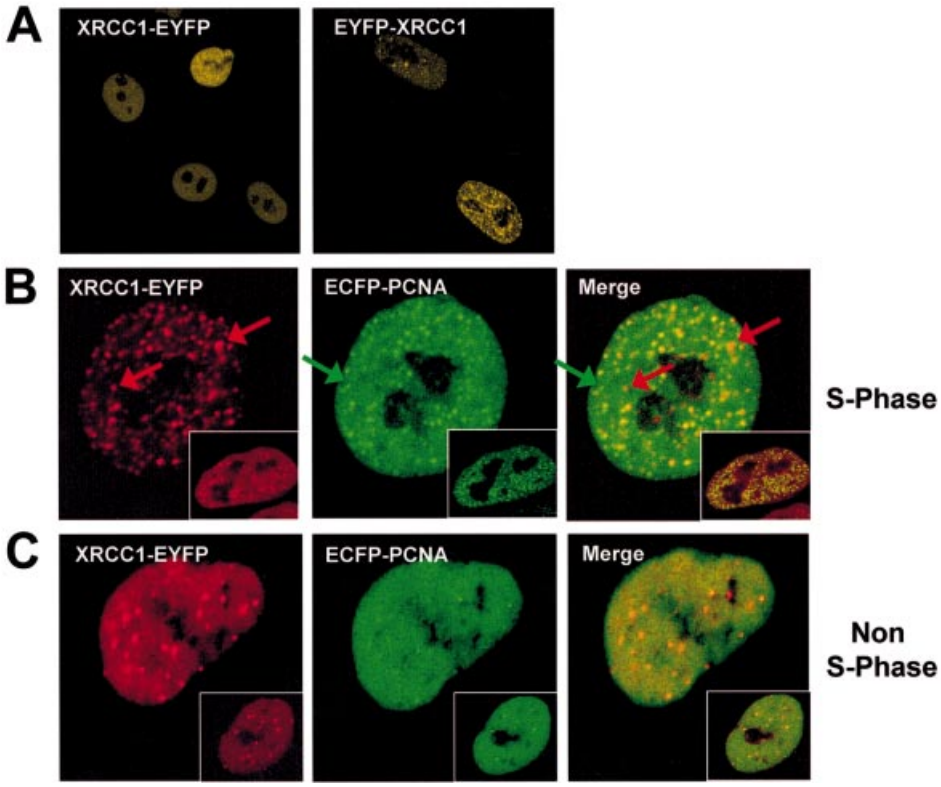

Figure 1. Localization of XRCC1 and PCNA in HeLa cells. (**A**) XRCC1 forms discrete foci. Constructs expressing either C- (left) or N-terminal (right) YFP-tagged human XRCC1 were transfected into HeLa cells. Fluorescently tagged protein was visualized using a Zeiss LSM 510 laser scanning microscope equipped with a Plan-Apochromate 63×/1.4 oil immersion objective (see Materials and Methods). (**B**) XRCC1 and PCNA co-localize in S phase human cells. The C-terminal YFP-tagged XRCC1 expression construct was co-transfected with a ECFP–PCNA expression construct and S phase cells with PCNA foci (which comprised ~10–20% of the cell population) were examined as above. The green arrow indicates foci with a higher degree of PCNA relative to XRCC1 and the orange arrows indicate foci with a higher level of XRCC1. (**C**) XRCC1 forms foci in non-S phase cells. The same constructs as in (B) were co-transfected and the cellular distribution of XRCC1 and PCNA was evaluated. Insets in (B) and (C) show a separate, representative cell.

RESULTS

XRCC1 forms discrete nuclear foci and co-localizes with PCNA

To investigate the biological functions of XRCC1, we designed a series of constructs that express fluorescently tagged XRCC1 fusion proteins and determined their *in vivo* cellular distribution. Upon transfection of either pXRCC1-EYFP or pEYFP-XRCC1 into HeLa cells, XRCC1 protein was found to reside primarily in the nucleus, independent of the position of the YFP tag (Fig. 1A). This intracellular localization pattern is consistent with the computational predictions of XRCC1 sorting (PSORT, http://www.psort.org/), the fact that XRCC1 maintains six consensus nuclear localization signals between residues 242 and 555 (PSORT) and previous reports (15,26). Moreover, the XRCC1 fusion protein was excluded from the nucleolus (the apparent 'black holes') and, in some cells, formed discrete nuclear foci (Fig. 1A).

While foci are associated with several biological processes, we explored the prospect that the XRCC1 foci were coincident with replication factories. PCNA was used as a marker for such factories, as it is an essential component of DNA replication and was the first protein identified in replication foci of S phase cells (27–29). Specifically, PCNA forms a homotrimeric ring around DNA, serving as a sliding clamp that tethers the polymerases (most notably DNA polymerase δ), as well as other replication-associated factors, to the DNA to ensure high processivity (30,31). Since green fluorescent protein (GFP)-tagged PCNA has been shown to form foci that co-localize completely with endogenous PCNA and with BrdU incorporation (i.e. sites of DNA replication) in S phase cells (32), we used a tagged PCNA construct to study both S and non-S phase stages in freely cycling living cells. Confocal microscopy of HeLa cells expressing both YFP-tagged XRCC1 and CFP-tagged PCNA revealed that up to 90% of the PCNA and XRCC1 foci co-localize in S phase cells (identified by PCNA foci; Fig. 1B). In non-S phase cells (defined as those with evenly distributed PCNA), XRCC1 formed varying numbers of discrete foci (up to 30) in ~80% of the cells (Fig. 1C). It is noteworthy that the relative intensity of the two proteins varied among the different foci and that some of the XRCC1 and PCNA foci did not coincide (see green and orange arrows in Fig. 1B).

This co-localization prompted us to examine the relative proximity of XRCC1 and PCNA using quantitative FRET analysis (33). FRET enables one to examine whether different proteins directly interact or, more precisely, whether the fluorescent tags (ECFP and EYFP) are within 100 Å of each

Table 2. FRET analysis indicates that XRCC1 and PCNA are in close proximity *in vivo*

Plasmid constructs co-transfected	$FRET_N = FRET/(I_1 \times I_3)^{1/2}$
XRCC1–ECFP and EYFP–PCNA[a]	0.16, 0.16, 0.15, 0.14, 0.12 0.06[b]
ECFP–PCNA and EYFP–PCNA	0.19, 0.16, 0.13, 0.12, 0.12 0.06[b]
UNG2–ECFP and UNG2–EYFP	0.05, 0.03 >95% of foci: <0.01[b]

The indicated plasmids (left) were co-transfected and the $FRET_N$ values were determined. $FRET_N$ represents the FRET value normalized against protein expression levels and measured as intensities (*I*) assigned in arbitrary units. FRET is calculated from the mean of *I* within a region of interest (ROI, a foci) containing more than 20 pixels. Within the ROI, all pixels had *I* values below 250, with *I* levels between 85 and 210 for the donor (ECFP) and 85 and 180 for the acceptor (EYFP). Data shown (right) indicate the highest (typically five, where available) and the lowest, yet positive, FRET values. The background level of $FRET_N$ (i.e. outside the foci) in each of the experiments was <0.01, which was also the maximum FRET in >95% of foci with co-localizing UNG2–ECFP and UNG2–EYFP proteins.

[a]XRCC1–EYFP and ECFP–PCNA produced similar FRET values.

[b]Lowest positive FRET value.

other (20). FRET occurs only when the intensity of emitted light measured in the presence of two fluorescently tagged proteins is greater than the emitted light from cells transfected with only blue- or yellow-tagged proteins (i.e. background levels; see Materials and Methods). The FRET values normalized against protein expression levels, $FRET_N$, are given in Table 2. Such scrutiny revealed that XRCC1 and PCNA fusion proteins exhibit an average $FRET_N$ of 0.15. This $FRET_N$ level is comparable to what was seen with the positive control ECFP–PCNA/EYFP–PCNA (PCNA is a known trimer) (34) and considerably higher than that of the negative (background) control UNG2–ECFP and UNG2–EYFP (a known monomer which interacts with PCNA in replication foci) (35). These observations suggest that XRCC1 and PCNA are likely associated directly *in vivo*. The $FRET_N$ for XRCC1–ECFP/XRCC1–EYFP was on average 0.55 and 0.26 within and outside XRCC1 foci, respectively, indicating that XRCC1 exists as a multimer *in vivo*.

XRCC1 and PCNA co-immunoprecipitate from whole cell extracts

To test further whether XRCC1 and PCNA coexist in a common protein complex *in vivo*, immunoprecipitation experiments were performed using 293T whole cell extracts treated with DNase I. As shown in Figure 2A, anti-PCNA antibody pulled down both PCNA and XRCC1 (see lane IP). However, we consistently found that co-immunoprecipitation of PCNA with anti-XRCC1 antibodies was less convincing (data not shown), perhaps reflecting inaccessibility of the antigenic epitope (to the XRCC1 antibody) in the context of the multi-protein complex or disruption of the XRCC1–PCNA interaction upon antibody association. The inability to immunoprecipitate proteins from cell extracts in a reciprocal manner has been seen with other protein partners as well (see for example 36).

As an alternative for assessing the complex nature of XRCC1 *in vivo*, we generated and employed a HeLa cell line

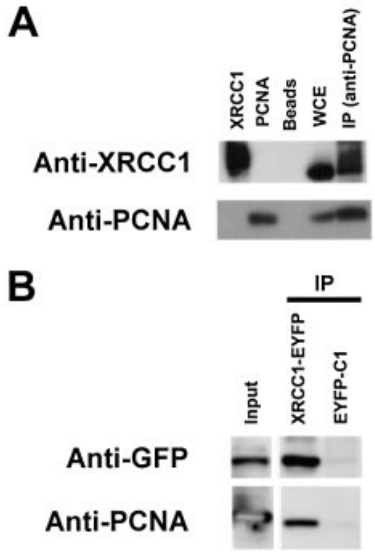

Figure 2. Co-immunoprecipitation of XRCC1 and PCNA. (**A**) Anti-PCNA antibody pulls down XRCC1. Whole cell extracts prepared from human 293T cells were subject to immunoprecipitation with anti-PCNA antibody as described in Materials and Methods. The precipitated proteins (IP) were fractionated by SDS–PAGE and probed with either anti-XRCC1 or anti-PCNA antibodies (as indicated) using standard immunoblotting techniques. XRCC1, purified recombinant XRCC1; PCNA, purified recombinant PCNA; beads, agarose bead control, without PCNA antibody; WCE, whole cell extract (~30 μg); IP, immunoprecipitant. (**B**) Anti-GFP antibody pulls down XRCC1–EYFP and PCNA. Cell extracts were prepared from HeLa cells stably expressing either XRCC1–EYFP or EYFP alone (EYFP-C1) and immunoprecipitations were performed with anti-GFP as described in Materials and Methods. The precipitated proteins (IP) were analyzed as above with the indicated antibodies. Input was 20% of the starting material from the XRCC1–EYFP extracts. Note that GFP alone is not shown, as it migrated at a much lower molecular weight than the XRCC1–EYFP fusion protein.

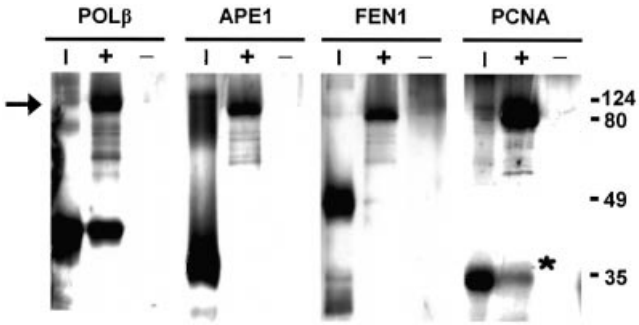

Figure 3. XRCC1 physically interacts with PCNA *in vitro*. Purified recombinant XRCC1 protein (+ lanes) was examined for physical association with purified recombinant POLβ, APE1, FEN1 or PCNA (as indicated) using the *in vitro* protein interaction assay described in Materials and Methods. Non-specific interactions of the four recombinant proteins with the affinity matrix were examined in the absence of XRCC1 (– lanes). Matrix bound proteins were analyzed by SDS–PAGE and silver staining (representative gel shown). I indicates the initial input for the POLβ, APE1, FEN1 and PCNA proteins. The asterisk denotes the location of the PCNA protein and the arrow indicates the position of the HIS- and S-tagged recombinant XRCC1 protein. Molecular weight protein standards are shown (in kDa) to the right.

stably expressing XRCC1–EYFP. Immunoprecipitation from these cell extracts using an antibody against GFP captured both the XRCC1–EYFP fusion protein and PCNA (Fig. 2B). Conversely, immunoprecipitation with the same antibody from extracts expressing only EYFP did not pull down PCNA.

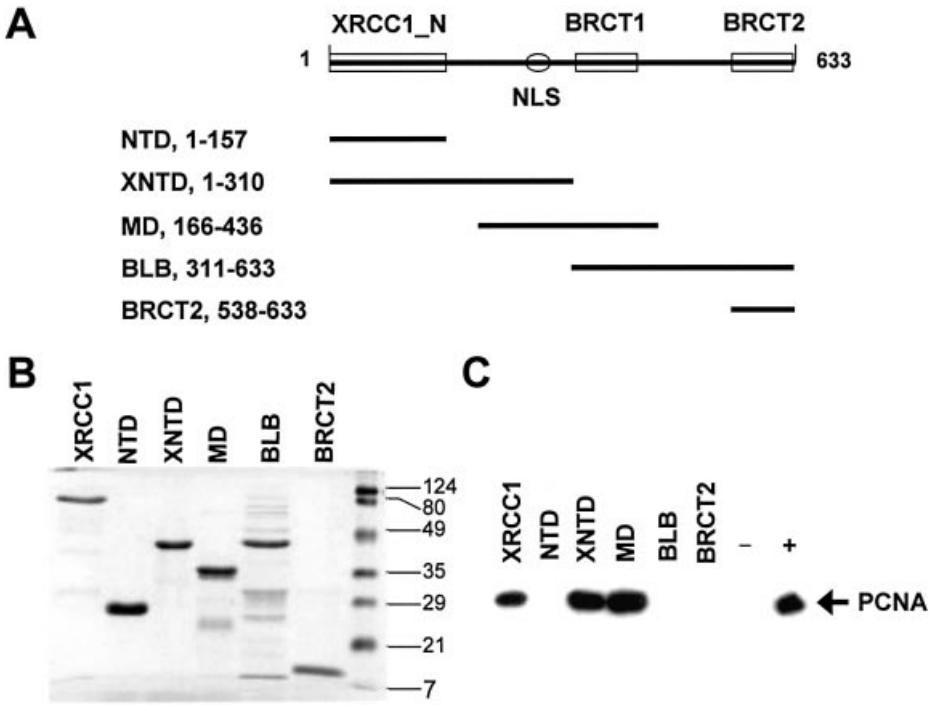

Figure 4. PCNA interacts with amino acids between 166 and 310 of XRCC1. (**A**) Schematic of the five human XRCC1 protein fragments. Names of protein fragments and the amino acid regions covered are indicated (see also Table 1). The locations of known functional domains and consensus sequences are denoted. XRCC1_N, N-terminal DNA binding and POLβ interaction domain; NLS, nuclear localization signals; BRCT1 and BRCT2, the central and C-terminal BRCT domains. (**B**) Purified XRCC1 recombinant proteins. Nickel-purified XRCC1 proteins were subjected to SDS–PAGE and stained with Coomassie brilliant blue. Full-length XRCC1 and protein fragments are indicated. Molecular weight protein standards (in kDa) are shown to the right. (**C**) PCNA interacts with the XNTD and MD fragments of XRCC1. Recombinant full-length XRCC1 protein (lane 1) or one of the XRCC1 fragments, NTD (lane 2), XNTD (lane 3), MD (lane 4), BLB (lane 5) and BRCT2 (lane 6), was bound to a Ni affinity matrix. Following incubation with purified PCNA (see Materials and Methods), matrix-associated proteins were separated by SDS–PAGE, transferred to a PVDF membrane and probed with anti-PCNA antibody. Lanes 7 (affinity matrix, with no XRCC1 protein) and 8 (150 ng purified PCNA) represent the negative and positive controls, respectively.

These complementary data further support the idea that XRCC1 and PCNA exist in a common protein complex.

XRCC1 physically interacts with PCNA

Using purified recombinant proteins, we next tested for a direct physical association between XRCC1 and PCNA. The human XRCC1 protein was both HIS tagged at the C-terminus and S peptide tagged at the N-terminus. Taking advantage of the S peptide tag, we bound purified XRCC1 to an S protein affinity matrix and examined several untagged human replication and repair-related proteins (APE1, POLβ, PCNA and FEN1) for direct interactions in pull-down assays. As shown in Figure 3, POLβ was strongly retained (i.e. ~50% of the input) by the XRCC1-bound matrix, but not the matrix alone, supporting previous findings that XRCC1 forms a stable complex with POLβ (5,6,37). In addition, we observed direct recovery of PCNA (~10% of the input) with the XRCC1-bound matrix, but not the matrix alone (Fig. 3), indicating a direct physical interaction between these two proteins, as supported by the FRET analysis (Table 2). In the solution studies here, we did not observe a strong interaction between XRCC1 and APE1, a previously demonstrated protein partner (8), nor did we see an association (i.e. consistently above background) with FEN1, a structure-specific endonuclease that operates in repair and replication (Fig. 3).

To define the PCNA-interacting region within XRCC1, we designed a series of XRCC1 protein fragments (Fig. 4A). Following partial purification (Fig. 4B), these fragments were immobilized onto Ni–NTA–agarose and examined for their ability to capture PCNA. In these studies, untagged PCNA was pulled down by full-length XRCC1, as well as by XNTD and MD, but not by NTD, BLB or BRCT2, as determined by anti-PCNA western blot analysis (Fig. 4C, see arrow). This experiment defines the region between the N-terminal and BRCT1 domains of XRCC1 (residues 166–310) as the interacting site for PCNA.

DISCUSSION

We report here that XRCC1 co-localizes with PCNA replication-specific foci, that these two proteins co-purify from human whole cell extracts and that XRCC1 physically interacts with PCNA *in vitro* via residues within 166–310 of XRCC1. Our finding brings the total number of XRCC1-interacting protein partners to at least eight (Fig. 5A and legend). While XRCC1 lacks a consensus PCNA interaction sequence (i.e. the PIP- or KA-box), other proteins without a consensus motif (e.g. Gadd45 and CAF1) have also been found to associate with PCNA (30,31). Moreover, the PCNA-interacting region found here (Fig. 5A) overlaps the portion of

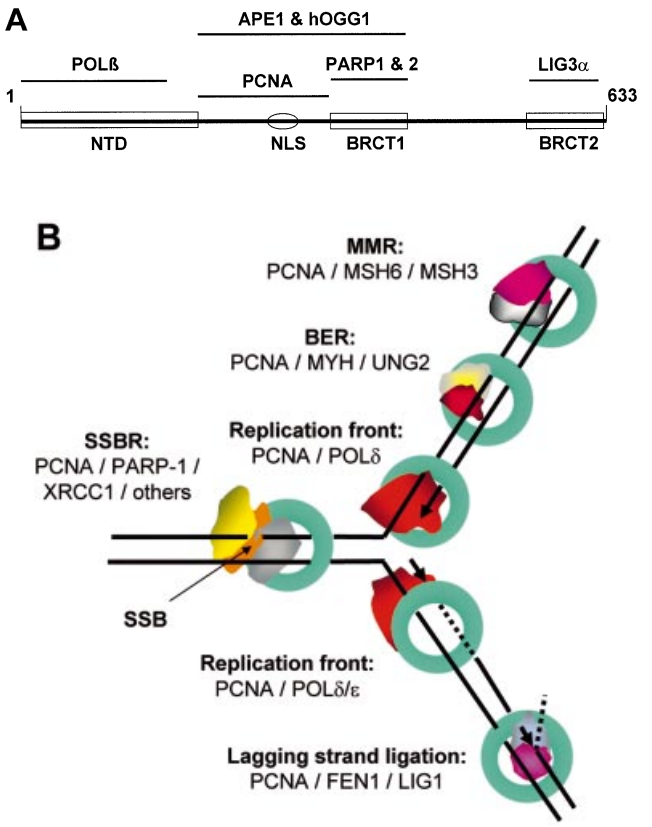

Figure 5. (**A**) Schematic of XRCC1 interacting regions and protein partners. Thus far, at least eight proteins (see text for details), including PCNA described in this work, have been found to directly interact with XRCC1. The regions that are responsible for these interactions, excluding PNK, have been assigned (see diagram). Note that TDP1 has not been shown to directly associate with XRCC1. (**B**) A model for 'replication-coupled repair'. XRCC1 is linked to DNA replication factories (i.e. foci) via its interaction with PCNA. This interaction increases the local concentration of XRCC1 (and potentially PARP-1) and facilitates rapid recognition and processing of SSBs, as XRCC1 functions to recruit other factors for repair. In other words, the coordination between replication and XRCC1 ensures proficient repair of SSBs and prevents DSB formation via damage-induced replication fork collapse and homologous recombination. Two other replication-linked pathways, namely post-replicative mismatch repair (MMR) and BER, operate on the newly synthesized strand behind the replication fork (see related reviews 49–53). Also shown is lagging strand ligation.

XRCC1 shown to interact with APE1 and OGG1 (8,13). Thus, elaborate mechanisms presumably exist to modulate the interactions of these various repair and regulatory proteins.

Both Caldecott and colleagues (15,17) and Kubota and Horiuchi (16) have suggested an S phase-specific role for XRCC1. In fact (as shown here in Fig. 1), Taylor *et al.* (15), using indirect immunofluorescence, observed S phase-specific XRCC1 foci, which they suggest are connected to RAD51 and DNA recombination. Our results indicate that such XRCC1 foci are associated with replication factories. Since Rad51 nuclear foci are seen exclusively in the S phase of undamaged human cells (38), the data in total may suggest that replication, repair and recombination are strategically intertwined. We propose that the S phase-specific XRCC1 foci reflect PCNA-directed sequestration of XRCC1 into strand break repair complexes that are associated with translocating DNA replication machines (Fig. 5B).

While we cannot exclude a role for XRCC1 in replication reinitiation, particularly following DNA damage induction (16), our 'replication-coupled repair' model is consistent with the observation that EM9 cells do not exhibit hypersensitivity to hydroxyurea, an agent used to evaluate the contribution of genetic factors to replication restart (H.-K. Wong and D.M. Wilson III, unpublished observations). In other words, XRCC1 does not appear to maintain a universal role in replication reinitiation. Moreover, since evidence suggests that XRCC1 is not a major participate in long patch, PCNA-dependent BER events (39), the XRCC1–PCNA foci seen here likely do not represent sites of 'conventional' long patch BER. While there is evidence that PCNA co-localizes to sites of atypical SSBs following DNA damage induction (26), these findings are not directly relevant to our studies, where exogenous DNA-damaging agent exposures were not employed. Nonetheless, they may suggest a cooperative role between XRCC1 and PCNA in certain SSBR processes outside of DNA replication.

A role for XRCC1 in specifically coordinating repair and replication is supported by the facts that XRCC1 mutant cells (i) exhibit an increased doubling time (from 13 to 16 h) (1) and (ii) display, as a hallmark, markedly elevated SCEs (40). In particular, spontaneous or EMS-induced SCEs are increased 7- to 12-fold in EM9 cells relative to their wild-type counterparts (1,41). While the precise molecular mechanism for SCEs is unclear, this genetic outcome is thought to result from homologous recombination repair of SSBs converted to DSBs upon replication fork collapse (42). PARP-1, for instance, has been shown to suppress SCEs by promoting efficient repair as opposed to regulating homologous recombination (43), and this protein, like XRCC1 (data within), has been linked to chromosome replication (44–46). On the other hand, POLβ$^{-/-}$ cells, which are also presumably defective in nick/gap DNA repair, exhibit no increase in spontaneous SCEs and only a mild (2-fold) increase in SCEs upon exposure to the alkylating agent MMS (47). Thus, the data in total suggest (i) unique functions for XRCC1 and PARP-1 in strand break repair, which we propose to be coordination of repair with replication, and (ii) that polymerases other than POLβ may function in XRCC1-associated SSBR during S phase.

Published data clearly indicate distinct roles for XRCC1 in the G_1 and S phases of the cell cycle (15,17). As described above, we propose a model (Fig. 5B) where in S phase XRCC1 specifically facilitates efficient SSBR through its interaction with PCNA (and progressing replication factories), prior to DNA replication arrest, fork collapse and DSB formation. In G_1, XRCC1 likely functions to coordinate direct BER/SSBR events (perhaps represented by the non-S phase foci seen in Fig. 1B). In particular, following PARP-1 relocalization and recruitment of XRCC1 to the strand break (26,48), XRCC1 operates to organize and 'scaffold' proteins such as POLβ, PNK and DNA ligase IIIα until repair is complete. Notably, among the small set of BER-related proteins analyzed here, the strongest *in vitro* XRCC1 interactor was POLβ (Fig. 3). Since we employed only recombinant proteins purified from bacteria, which do not contain eukaryotic-like post-translational modifications, this finding may suggest that XRCC1 is largely unmodified in G_1 and, in this state, more proficient at interacting with POLβ, and potentially DNA ligase IIIα, to mediate nick and gap DNA repair. Whether XRCC1

undergoes post-translational modification upon entry into S phase or following exposure to a DNA-damaging agent that alters its ability (or affinity) to specifically interact with proteins in repair, replication and/or recombination (such as PARP-1, PCNA and RAD51) awaits further investigation. Importantly, evidence exists for phosphorylation of the XRCC1 polypeptide (16).

ACKNOWLEDGEMENTS

We are grateful to Dr Larry Thompson (Lawrence Livermore National Laboratory) for providing the XRCC1 cDNA. We thank Knut Lauritzen and Bruno Monterotti (Department of Cancer Research and Molecular Medicine, Norwegian University of Science and Technology) for technical assistance. This work was supported in part by The Research Council of Norway (M.O.) and by National Institutes of Health research grants (GM57479 and ES012521 to A.E.T).

REFERENCES

1. Thompson,L.H., Brookman,K.W., Dillehay,L.E., Carrano,A.V., Mazrimas,J.A., Mooney,C.L. and Minkler,J.L. (1982) A CHO-cell strain having hypersensitivity to mutagens, a defect in DNA strand-break repair and an extraordinary baseline frequency of sister-chromatid exchange. *Mutat. Res.*, **95**, 427–440.
2. Dillehay,L.E., Thompson,L.H. and Carrano,A.V. (1984) DNA-strand breaks associated with halogenated pyrimidine incorporation. *Mutat. Res.*, **131**, 129–136.
3. Thompson,L.H., Brookman,K.W., Jones,N.J., Allen,S.A. and Carrano,A.V. (1990) Molecular cloning of the human XRCC1 gene, which corrects defective DNA strand break repair and sister chromatid exchange. *Mol. Cell. Biol.*, **10**, 6160–6171.
4. Caldecott,K.W., McKeown,C.K., Tucker,J.D., Ljungquist,S. and Thompson,L.H. (1994) An interaction between the mammalian DNA repair protein XRCC1 and DNA ligase III. *Mol. Cell. Biol.*, **14**, 68–76.
5. Caldecott,K.W., Aoufouchi,S., Johnson,P. and Shall,S. (1996) XRCC1 polypeptide interacts with DNA polymerase β and possibly poly (ADP-ribose) polymerase and DNA ligase III is a novel molecular 'nick-sensor' *in vitro*. *Nucleic Acids Res.*, **24**, 4387–4394.
6. Kubota,Y., Nash,R.A., Klungland,A., Schar,P., Barnes,D.E. and Lindahl,T. (1996) Reconstitution of DNA base excision-repair with purified human proteins: interaction between DNA polymerase β and the XRCC1 protein. *EMBO J.*, **15**, 6662–6670.
7. Marintchev,A., Mullen,M.A., Maciejewski,M.W., Pan,B., Gryk,M.R. and Mullen,G.P. (1999) Solution structure of the single-strand break repair protein XRCC1 N-terminal domain. *Nature Struct. Biol.*, **6**, 884–893.
8. Vidal,A.E., Boiteux,S., Hickson,I.D. and Radicella,J.P. (2001) XRCC1 coordinates the initial and late stages of DNA abasic site repair through protein–protein interactions. *EMBO J.*, **20**, 6530–6539.
9. Whitehouse,C.J., Taylor,R.M., Thistlethwaite,A., Zhang,H., Karimi-Busheri,F., Lasko,D.D., Weinfeld,M. and Caldecott,K.W. (2001) XRCC1 stimulates human polynucleotide kinase activity at damaged DNA termini and accelerates DNA single-strand break repair. *Cell*, **104**, 107–117.
10. Plo,I., Liao,Z.Y., Barcelo,J.M., Kohlhagen,G., Caldecott,K.W., Weinfeld,M. and Pommier,Y. (2003) Association of XRCC1 and tyrosyl DNA phosphodiesterase (Tdp1) for the repair of topoisomerase I-mediated DNA lesions. *DNA Repair (Amst.)*, **2**, 1087–1100.
11. Masson,M., Niedergang,C., Schreiber,V., Muller,S., Menissier-de Murcia,J. and de Murcia,G. (1998) XRCC1 is specifically associated with poly(ADP-ribose) polymerase and negatively regulates its activity following DNA damage. *Mol. Cell. Biol.*, **18**, 3563–3571.
12. Schreiber,V., Ame,J.C., Dolle,P., Schultz,I., Rinaldi,B., Fraulob,V., Menissier-de Murcia,J. and de Murcia,G. (2002) Poly(ADP-ribose) polymerase-2 (PARP-2) is required for efficient base excision DNA repair in association with PARP-1 and XRCC1. *J. Biol. Chem.*, **277**, 23028–23036.
13. Marsin,S., Vidal,A.E., Sossou,M., Menissier-de Murcia,J., Le Page,F., Boiteux,S., de Murcia,G. and Radicella,J.P. (2003) Role of XRCC1 in the coordination and stimulation of oxidative DNA damage repair initiated by the DNA glycosylase hOGG1. *J. Biol. Chem.*, **278**, 44068–44074.
14. Yamane,K., Katayama,E. and Tsuruo,T. (2000) The BRCT regions of tumor suppressor BRCA1 and of XRCC1 show DNA end binding activity with a multimerizing feature. *Biochem. Biophys. Res. Commun.*, **279**, 678–684.
15. Taylor,R.M., Moore,D.J., Whitehouse,J., Johnson,P. and Caldecott,K.W. (2000) A cell cycle-specific requirement for the XRCC1 BRCT II domain during mammalian DNA strand break repair. *Mol. Cell. Biol.*, **20**, 735–740.
16. Kubota,Y. and Horiuchi,S. (2003) Independent roles of XRCC1's two BRCT motifs in recovery from methylation damage. *DNA Repair (Amst.)*, **2**, 407–415.
17. Taylor,R.M., Thistlethwaite,A. and Caldecott,K.W. (2002) Central role for the XRCC1 BRCT I domain in mammalian DNA single-strand break repair. *Mol. Cell. Biol.*, **22**, 2556–2563.
18. Aas,P.A., Otterlei,M., Falnes,P.O., Vagbo,C.B., Skorpen,F., Akbari,M., Sundheim,O., Bjoras,M., Slupphaug,G., Seeberg,E. *et al.* (2003) Human and bacterial oxidative demethylases repair alkylation damage in both RNA and DNA. *Nature*, **421**, 859–863.
19. Matyus,L. (1992) Fluorescence resonance energy transfer measurements on cell surfaces. A spectroscopic tool for determining protein interactions. *J. Photochem. Photobiol. B*, **12**, 323–337.
20. Baynton,K., Otterlei,M., Bjoras,M., von Kobbe,C., Bohr,V.A. and Seeberg,E. (2003) WRN interacts physically and functionally with the recombination mediator protein RAD52. *J. Biol. Chem.*, **278**, 36476–36486.
21. Xia,Z. and Liu,Y. (2001) Reliable and global measurement of fluorescence resonance energy transfer using fluorescence microscopes. *Biophys. J.*, **81**, 2395–2402.
22. Levin,D.S., Bai,W., Yao,N., O'Donnell,M. and Tomkinson,A.E. (1997) An interaction between DNA ligase I and proliferating cell nuclear antigen: implications for Okazaki fragment synthesis and joining. *Proc. Natl Acad. Sci. USA*, **94**, 12863–12868.
23. Erzberger,J.P., Barsky,D., Scharer,O.D., Colvin,M.E. and Wilson,D.M.,III (1998) Elements in abasic site recognition by the major human and *Escherichia coli* apurinic/apyrimidinic endonucleases. *Nucleic Acids Res.*, **26**, 2771–2778.
24. Nguyen,L.H., Barsky,D., Erzberger,J.P. and Wilson,D.M.,III (2000) Mapping the protein-DNA interface and the metal-binding site of the major human apurinic/apyrimidinic endonuclease. *J. Mol. Biol.*, **298**, 447–459.
25. Lee,B.I. and Wilson,D.M.,III (1999) The RAD2 domain of human exonuclease 1 exhibits 5′ to 3′ exonuclease and flap structure-specific endonuclease activities. *J. Biol. Chem.*, **274**, 37763–37769.
26. Okano,S., Lan,L., Caldecott,K.W., Mori,T. and Yasui,A. (2003) Spatial and temporal cellular responses to single-strand breaks in human cells. *Mol. Cell. Biol.*, **23**, 3974–3981.
27. Bravo,R. and Macdonald-Bravo,H. (1985) Changes in the nuclear distribution of cyclin (PCNA) but not its synthesis depend on DNA replication. *EMBO J.*, **4**, 655–661.
28. Celis,J.E. and Celis,A. (1985) Cell cycle-dependent variations in the distribution of the nuclear protein cyclin proliferating cell nuclear antigen in cultured cells: subdivision of S phase. *Proc. Natl Acad. Sci. USA*, **82**, 3262–3266.
29. Prelich,G., Tan,C.K., Kostura,M., Mathews,M.B., So,A.G., Downey,K.M. and Stillman,B. (1987) Functional identity of proliferating cell nuclear antigen and a DNA polymerase-delta auxiliary protein. *Nature*, **326**, 517–520.
30. Warbrick,E. (2000) The puzzle of PCNA's many partners. *Bioessays*, **22**, 997–1006.
31. Maga,G. and Hubscher,U. (2003) Proliferating cell nuclear antigen (PCNA): a dancer with many partners. *J. Cell Sci.*, **116**, 3051–3060.
32. Leonhardt,H., Rahn,H.P., Weinzierl,P., Sporbert,A., Cremer,T., Zink,D. and Cardoso,M.C. (2000) Dynamics of DNA replication factories in living cells. *J. Cell Biol.*, **149**, 271–280.
33. Sekar,R.B. and Periasamy,A. (2003) Fluorescence resonance energy transfer (FRET) microscopy imaging of live cell protein localizations. *J. Cell Biol.*, **160**, 629–633.
34. Brand,S.R., Bernstein,R.M. and Mathews,M.B. (1994) Trimeric structure of human proliferating cell nuclear antigen. Implications for enzymatic function and autoantibody recognition. *J. Immunol.*, **153**, 3070–3078.
35. Otterlei,M., Warbrick,E., Nagelhus,T.A., Haug,T., Slupphaug,G., Akbari,M., Aas,P.A., Steinsbekk,K., Bakke,O. and Krokan,H.E. (1999)

Post-replicative base excision repair in replication foci. *EMBO J.*, **18**, 3834–3844.
36. von Kobbe,C., Karmakar,P., Dawut,L., Opresko,P., Zeng,X., Brosh,R.M.,Jr, Hickson,I.D. and Bohr,V.A. (2002) Colocalization, physical and functional interaction between Werner and Bloom syndrome proteins. *J. Biol. Chem.*, **277**, 22035–22044.
37. Marintchev,A., Gryk,M.R. and Mullen,G.P. (2003) Site-directed mutagenesis analysis of the structural interaction of the single-strand-break repair protein, X-ray cross-complementing group 1, with DNA polymerase β. *Nucleic Acids Res.*, **31**, 580–588.
38. Tashiro,S., Kotomura,N., Shinohara,A., Tanaka,K., Ueda,K. and Kamada,N. (1996) S phase specific formation of the human Rad51 protein nuclear foci in lymphocytes. *Oncogene*, **12**, 2165–2170.
39. Cappelli,E., Taylor,R., Cevasco,M., Abbondandolo,A., Caldecott,K. and Frosina,G. (1997) Involvement of XRCC1 and DNA ligase III gene products in DNA base excision repair. *J. Biol. Chem.*, **272**, 23970–23975.
40. Thompson,L.H. and West,M.G. (2000) XRCC1 keeps DNA from getting stranded. *Mutat. Res.*, **459**, 1–18.
41. Pinero,J. and Cortes,F. (1993) Abnormally high incidence of SCE in three successive cell cycles in the CHO mutant EM9 as detected by a three-way immunoperoxidase differential staining. *Mutat. Res.*, **292**, 205–211.
42. Arnaudeau,C., Lundin,C. and Helleday,T. (2001) DNA double-strand breaks associated with replication forks are predominantly repaired by homologous recombination involving an exchange mechanism in mammalian cells. *J. Mol. Biol.*, **307**, 1235–1245.
43. Schultz,N., Lopez,E., Saleh-Gohari,N. and Helleday,T. (2003) Poly(ADP-ribose) polymerase (PARP-1) has a controlling role in homologous recombination. *Nucleic Acids Res.*, **31**, 4959–4964.
44. Simbulan-Rosenthal,C.M., Rosenthal,D.S., Boulares,A.H., Hickey,R.J., Malkas,L.H., Coll,J.M. and Smulson,M.E. (1998) Regulation of the expression or recruitment of components of the DNA synthesome by poly(ADP-ribose) polymerase. *Biochemistry*, **37**, 9363–9370.
45. Dantzer,F., Nasheuer,H.P., Vonesch,J.L., de Murcia,G. and Menissier-de Murcia,J. (1998) Functional association of poly(ADP-ribose) polymerase with DNA polymerase alpha-primase complex: a link between DNA strand break detection and DNA replication. *Nucleic Acids Res.*, **26**, 1891–1898.
46. Frouin,I., Maga,G., Denegri,M., Riva,F., Savio,M., Spadari,S., Prosperi,E. and Scovassi,A.I. (2003) Human proliferating cell nuclear antigen, poly(ADP-ribose) polymerase-1 and p21waf1/cip1. A dynamic exchange of partners. *J. Biol. Chem.*, **278**, 39265–39268.
47. Sobol,R.W., Kartalou,M., Almeida,K.H., Joyce,D.F., Engelward,B.P., Horton,J.K., Prasad,R., Samson,L.D. and Wilson,S.H. (2003) Base excision repair intermediates induce p53-independent cytotoxic and genotoxic responses. *J. Biol. Chem.*, **278**, 39951–39959.
48. El Khamisy,S.F., Masutani,M., Suzuki,H. and Caldecott,K.W. (2003) A requirement for PARP-1 for the assembly or stability of XRCC1 nuclear foci at sites of oxidative DNA damage. *Nucleic Acids Res.*, **31**, 5526–5533.
49. Lu,A.L., Li,X., Gu,Y., Wright,P.M. and Chang,D.Y. (2001) Repair of oxidative DNA damage: mechanisms and functions. *Cell Biochem. Biophys.*, **35**, 141–170.
50. Marti,T.M., Kunz,C. and Fleck,O. (2002) DNA mismatch repair and mutation avoidance pathways. *J. Cell. Physiol.*, **191**, 28–41.
51. Mitra,S., Izumi,T., Boldogh,I., Bhakat,K.K., Hill,J.W. and Hazra,T.K. (2002) Choreography of oxidative damage repair in mammalian genomes. *Free Radic. Biol. Med.*, **33**, 15–28.
52. Fortini,P., Pascucci,B., Parlanti,E., D'Errico,M., Simonelli,V. and Dogliotti,E. (2003) 8-Oxoguanine DNA damage: at the crossroad of alternative repair pathways. *Mutat. Res.*, **531**, 127–139.
53. Caldecott,K.W. (2003) XRCC1 and DNA strand break repair. *DNA Repair (Amst.)*, **2**, 955–969.